International Journal of
INTELLIGENT SYSTEMS AND APPLICATIONS IN ENGINEERING
ISSN:2147-6799 www.ijisae.org Original Research Paper

Wind Effects on Non-Regular Building Shapes as a Function of Velocity Angle: A Computational Fluid Dynamics (CFD) Study

Pankaj N. Pagare[1]*, Sunil Y. Kute[2]

Submitted: 13/03/2024 **Revised**: 29/04/2024 **Accepted**: 07/05/2024

Abstract: This study investigates how different velocity angles affect the aerodynamics of irregular shape structures, focusing on Y, L, and + configurations. Its main goal is to evaluate how varying velocity angles influence the aerodynamic characteristics of these designs. Additionally, it explores the impact of mesh finite element density on result accuracy. Computational Fluid Dynamics (CFD) is employed to analyse the effects of 50 m/s wind speed on these buildings, providing a robust solver and extensive pre and post-processing capabilities for a comprehensive study. Pre-processing involves geometry modeling, meshing, material specification, and boundary condition setup. The k-ε model and momentum, fluid energy, and continuity equations are utilised for response calculation. Post-processing includes the examination of velocity profiles, path lines, pressure distributions, and forces. This research contributes to understanding how building shape, wind angles, and mesh density influence fluid dynamics around structures, aiding in the development of more slender, efficient, and resilient structures in the face of climate change.

Keywords: *Wind load, Tall buildings, Computational Fluid Dynamics, Irregular Shapes, Velocity, k- ε model*

Nomenclature

ρ	Density	$\tilde{G}_k$	Generation of turbulent kinetic energy
k	Turbulent kinetic energy	Y_k	Turbulent dissipation rate due to molecular viscosity
t	Time	S_k	Turbulent dissipation rate due to turbulence-transport processes
u_i	Velocity components in the i direction	σ_k	Turbulent Prandtl number for turbulent kinetic energy
x_i	Spatial coordinates in the i direction	E_{ij}	Rate of strain tensor
x_j	Spatial coordinates in the y direction	$\tilde{G}_k$	Generation of turbulent kinetic energy due to mean velocity gradients
μ_t	Turbulent viscosity	Y_k	Dissipation of turbulent kinetic energy due to turbulence
Γ_k	Turbulent diffusivity of k	S_k	Source/sink term for turbulent kinetic energy due to other physical processes

1. Introduction

Towering structures maximise land use while serving as iconic symbols of a country's prosperity in an era of rapidly increasing urbanisation. However, as buildings get taller, it becomes increasingly challenging to keep stable against external factors like wind pressure. The dynamic and ever-changing nature of wind impacts posed a significant problem for structural engineers. The Gust Factor Method is a widely used technique for assessing various wind loads. It is a comparable static wind load method. In addition to wind and turbulence, it considers structural height [1].

The behavior of wind is complex and flexible. Many types of structures and barriers change flow conditions, which influence the flow [2]. The wind around Earth is turbulent due to eddies of various magnitudes and rotating patterns. Earth-surface interactions, especially in the lower atmosphere, cause powerful winds to gust. Wind speeds rise over time, while gustiness diminishes with height [3]. For these complexities, CFD is a viable alternative to wind tunnel investigations. CFD uses the Navier-Stokes equations to solve fluid flow issues [4]. Due to advances in computer technology, sophisticated simulations can now be done efficiently, making CFD essential in wind engineering.

[1] *K. K. Wagh Institute of Eng. Edu. & Research, Nasik – 422003, INDIA*
ORCID ID: 0009-0004-6897-4159
[2] *K. K. Wagh Institute of Eng. Edu. & Research, Nasik – 422003, INDIA*
ORCID ID: 0000-0002-7393-4344
** Corresponding Author Email: pankajpagare13@email.com*

It is used in nature ventilation research, building heat transfer, pollutant dispersion, and pedestrian safety [5]. The CFD software improved its transonic and turbulent flow modelling. The study showed the accuracy of software in atmospheric boundary layer dynamics [6].

Tall structures are designed to withstand winds via lateral stiffness rather than sheer structural strength. However, modern methods need an understanding of effect of wind on non-uniform structures [7]. CFD analysis is necessary to understand the impact of mesh precision and velocity angles on the turbulent wind behaviour of irregular objects. Given changing urban contexts and worldwide building height constraints, understanding the complex influence of wind on diverse building forms is essential to ensure the structural stability and safety of these architectural wonders [8]. Dynamic façades and aerodynamic shape adjustment have helped to overcome wind fluctuations. Studies show that Artificial Intelligence (AI) agents and sophisticated morphing technologies can reduce wind damage to civil infrastructure. This new technology allows structures to dynamically adjust in real time, optimising aerodynamic configurations for efficiency and stability. Artificial intelligence and other new technologies in civil engineering helped create a flexible, strong, and sustainable infrastructure that could bear wind and other dynamic factors [9]. Visual analysis using fuzzy visibility findings to detect tall structures placements is the recommended strategy, taking practical and aesthetic factors into account. Fuzzy logic, a mathematical tool for controlling uncertainty and imprecision, is used to account for subjective evaluations of visibility and attractiveness [10]. In 2018, scalar dispersion in an array of uniformly raised buildings with flow was compared to that in an array with a building. It was observed that when the wind directly confronted the highest side of the structure, it responded more to minute-to-minute wind direction changes [11]. Thus, wind tunnel model configuration must be carefully considered to obtain a symmetrical flow field. It also suggested that significant temporal averaging is needed for Large-Eddy Simulation (LES) to converge to nearly symmetric mean fields.

Wind direction and speed are important aspects to take into account while analysing the wind flow characteristics of tall buildings. To lower the damping capacity, the strength and design criteria were investigated in the research on the impacts of wind loads on thin structures. The design load and vibration were discovered as a result. It produced the perfect blend of needs for flexibility, serviceability, and durability [12]. Other approaches, such as gust factor and wind tunnel techniques, are also used to calculate the shear and deflection of tall buildings and to produce reliable results. Although the dynamic-wind technique or gust factor methodology described in IS 875-2015 [13] was considered to offer a significant margin of safety, the wind tunnel experiments produced more accurate findings that were more by the real site circumstances. An investigation into the impacts of various geometric plan configurations—Square, Circular, Hexagon, and Octagon—on the force coefficients of tall structures with equal plan areas was the goal of an experimental project [14]. A three-dimensional wind flow scenario surrounding a tall building was generated using the CFD Code Fluent/Gambit in order to assess the effects of wind. Then, a numerical computation was performed to determine the pressure coefficients and the wake zone around the structure. During the investigation, the wind pressure coefficient was maximum for tall structures with square plan shapes but reduced for circular plan shapes. The octagonal plan form was shown to be more successful than the hexagonal plan shape in decreasing the wind pressure coefficient when tall buildings have prominent windward sides. The aerodynamics of different building forms were examined using wind tunnel research to determine whether it would be possible to capture wind energy produced by airflow over built regions [15,16]. The study calculated surface pressure and flow velocity by systematically examining high-rise buildings with flat roofs, tilted roofs, low-rise roofs, and industrial buildings with slanted roofs. Individual building shapes were investigated from numerous flow angles. The disruptive effects of building arrangements were also explored. For each design, roof velocities were measured at different building heights. Depending on structural design, surface pressures on one or two rings and the roof were evaluated at different heights. In addition to wind tunnel testing, the study used CFD models to compare the two data sets.

Wind tunnel testing was utilised to analyse cladding loads for a high-rise building in the commercial sector of Chongqing Municipality. The structure was 295m tall. External pressures on the structures were calculated using a rigid model. The wind tunnel investigations provided vital data on wind pressure distribution over building surfaces, including interfering and independent situations. The FLUENT Code was used for CFD analysis to validate and improve wind tunnel results. The study used the Reliable k-′ turbulence model to simulate stable three-dimensional turbulent flow. The accuracy and dependability of computer models in duplicating wind pressures on high-rise building surfaces were examined by comparing CFD findings to wind tunnel tests. Wind tunnel testing was popular in tall skyscraper development. However, computational fluid dynamics analysis is being used to evaluate design early in locations with minimum to moderate turbulence. Both CFD analysis and wind tunnel testing give reliable assessments, CFD analysis is more commonly used due to its efficiency and affordability. In contrast to wind tunnel testing data, CFD analysis provided direct and thorough reporting. It excels at resolving unstable gusts and eddies, making it useful for investigating highly turbulent winds [17]. The

ability of CFD to avoid scaling and probing ensures data integrity, which is a significant advantage. Apart from other approaches, CFD analysis shows data with high resolution and visual clarity and show flow patterns in a way that is clear and appealing [18]. Designers were able to communicate complex information by understanding the aerodynamics of tall structures. CFD is a specialist science that studies complex fluid-liquid-solid-gas interactions. This field employed computational techniques to study fluid flow dynamics, specifically solid-air interactions. The CFX mode of ANSYS was used in CFD to calculate streamlines and pressure coefficients. The CFD technique included essential components to understand fluid dynamics. A detailed formulation and a mathematical model were built to accurately represent the system before solving the flow problem. The fluid dynamics simulation environment was created by establishing starting and boundary conditions. It was very important to make a mesh, which is a discretised model of the computing area. After laying the groundwork, a simulation plan solved the governing equations using numerical methods and algorithms. For the simulation to work, input the essential files and settings. The simulation was then run, and the results were carefully checked for correctness and completeness [19]. The thorough analysis ensured data correctness and conformity with fluid dynamics.

2. Material Properties and Study Area

CFD is used to explore the aerodynamics of a non-rectangular building in 50 m/s wind speed. The research sought to understand the velocity, pressure, and forces of these conditions. The study used Ansys Design and CFX 2022 R1. Simulations of fluid flow and building structures using ANSYS CFX evaluated pressure distribution, velocity profile, and wind force magnitude. In complex geometries, ANSYS CFX was capable of analysing both incompressible and compressible fluid flow as well as heat transmission.

2.1. Material Properties

The understanding of the interaction between air and concrete relies on the characteristics of the materials involved. The molar mass provided molecular weights and structure information about a material. The ratio of mass to volume, and density, affected aerodynamics and structural stability, controlling how materials reacted to external forces. The specific heat capacity of a material provided a quantitative measure of its thermal response, which was crucial for understanding thermal properties. Standard temperature and pressure allow reliable analysis in many scenarios. Thermal expansion demonstrated how temperature affected the size of material, while specific enthalpy assessed its energy. Building design, study, and evaluation require structural integrity, thermal control, and performance.

Table 1. Material properties of building

Material Properties	***Details of Air***	***Details of Concrete***
Molar Mass	28.96 kg/mol	1 kg/mol
Density	1.185 kg/m^3	2300 kg/m^3
Specific Heat Capacity	1.0044 E+03 J/kgK	8.80E+02 J/kgK
Ref. Temp.	25 ^{o}C	25 ^{o}C
Ref. Pressure	1 atm	-
Ref. Specific Enthalpy	0 J/kg	0 J/kg
Thermal Expansion	0.003356 K^{-1}	-
Molar Mass	28.96 kg/mol	1 kg/mol

The material properties outlined in Table 1 play a vital role in optimising structural design, thermal control, and evaluating building performance. The molar mass, density, specific heat capacity, thermal expansion, reference temperature, pressure, and specific enthalpy were crucial factors in understanding material behavior.

2.2. Basic Wind Speed

When constructing buildings and structures in compliance with Indian Standard code IS 875-2015, reference wind speed, also referred to as basic wind speed is the essential parameter to take into account [11, 13]. Statistics and historical records were used to establish basic wind velocities over 50 years. The annual likelihood of wind speeds exceeding this is 2%. Every wind zone in India had a baseline wind speed, from Zone I to Zone V. Zone V had the highest wind speeds and Zone I had the lowest. The wind speeds in Zone V reach a velocity of 60 m/s, whereas Zone I averages 33 m/s. The study set the maximum wind speed in Maharashtra at 50 m/s based on the criteria outlined in IS 875-2015.

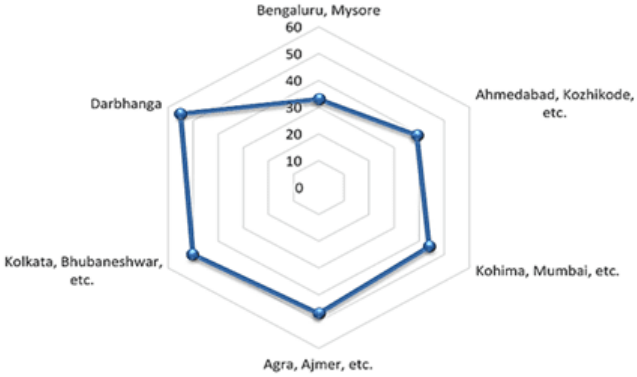

Fig. 1. Basic Wind Speeds in Important Indian Cities as per IS 875-2015 [13

Fig.1 shows the basic wind speeds of a number of important

cities located in various zones of India. Local environmental factors, climatic conditions, and geographic characteristics are considered while determining fundamental wind speeds. Strong winds frequently affected coastal communities, resulting in high wind speeds in open regions and adjacent water. Inland areas with flat or rising plateaus have milder wind patterns. The findings highlighted the significance of geometrical designs in guaranteeing building safety and structural integrity in various urban situations.

3. Research Methodology

The study examined the generated contours and streamlines to evaluate the fluid-structure interaction, which was necessary to comply with the coding requirement, and then confirmed the results [20]. The method analysed the influence of wind on low-rise structures and streamlined investigations by utilising traditional k- ε, k-ω, and SST k-ω models.

3.1. Standard k - ε model

The k-ε model, a two-equation computational fluid dynamics model, replicated flow features in streamlined flow circumstances. A uniform wind streamline velocity of 50 m/s was employed. Unlike the SST k-ω model, this model had a less noticeable streamline. For optimal kinetic energy efficiency,

$$\frac{\partial(\rho k)}{\partial t} + \frac{\partial(\rho k u_i)}{\partial x_i} = \frac{\partial}{\partial x_j}\left[\frac{\mu_t}{\sigma_k}\frac{\partial k}{\partial x_j}\right] + 2\mu_t E_{ij}E_{ij} - \rho\varepsilon \qquad (1)$$

The k-ε model Eq. (1), has been extensively utilised as a turbulence model since its early conception. It is simple and computationally efficient, making it suitable for many technical applications. The model solved two transport equations: one for turbulent kinetic energy and another for turbulent dissipation rate. The two-equation k-ε CFD model is being selected due to its capability to accurately replicate streamlined flow features. This model solve turbulent kinetic energy (k) and dissipation rate (ε) equations, making it ideal for wall-restricted flows. The approach produced vague results for complex turbulent flows, despite being computationally efficient. It was frequently utilised because to its simplicity and suitability for high Reynolds number flow.

3.2. Standard k – ω model

The analysis of streamline flow conditions at low Reynolds numbers utilised the two-equation model. The k-ω model was found to provide the most accurate answer for open channel flow concerns. For optimal kinetic energy efficiency,

$$\frac{\partial(\rho k)}{\partial t} + \frac{\partial(\rho\varepsilon u_i)}{\partial x_i} = \frac{\partial}{\partial x_j}\left[\Gamma_k \frac{\partial k}{\partial x_j}\right] + G_k - Y_k + S_k \qquad (2)$$

The k-ω model Eq. (2), performed better than the k-ε model as it addressed the limitations of the latter. The k-ω model eliminates the necessity to calculate for ε when ω (specific turbulence dissipation rate) is explicitly taken into consideration. This approach was more resilient and well-suited for complex flow conditions, including split and whirling flows. The k-ω model outperformed the k-ε model near walls and provided more accurate forecasts in specific conditions. However, pressure gradients and changing flows caused problems.

3.3. SST k – ω model

In unfavorable pressure gradients, the Shear Stress Transport (SST) approach improved flow separation prediction. To

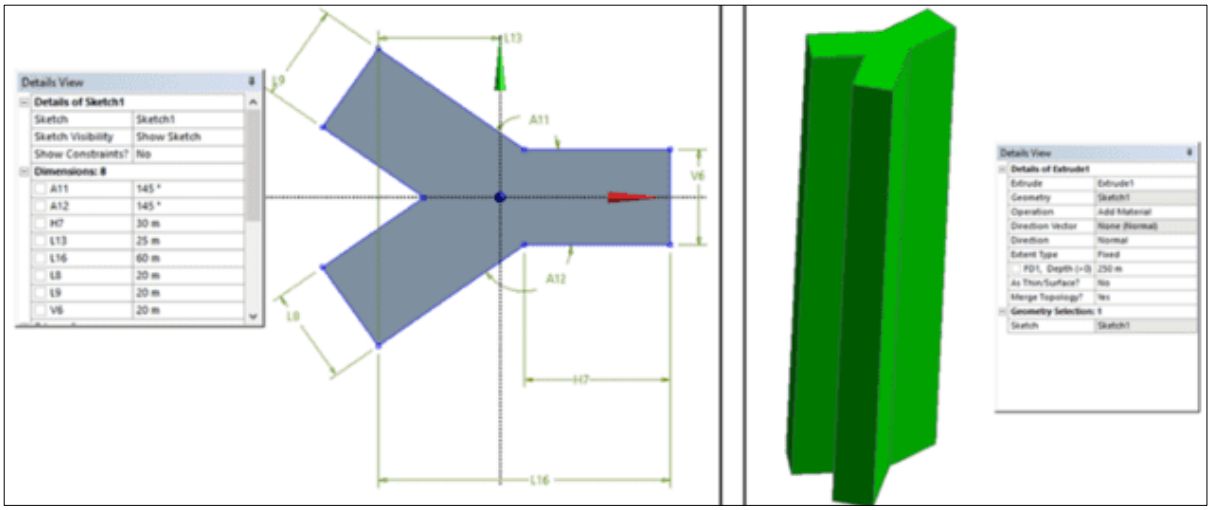

(a) Y- Shape

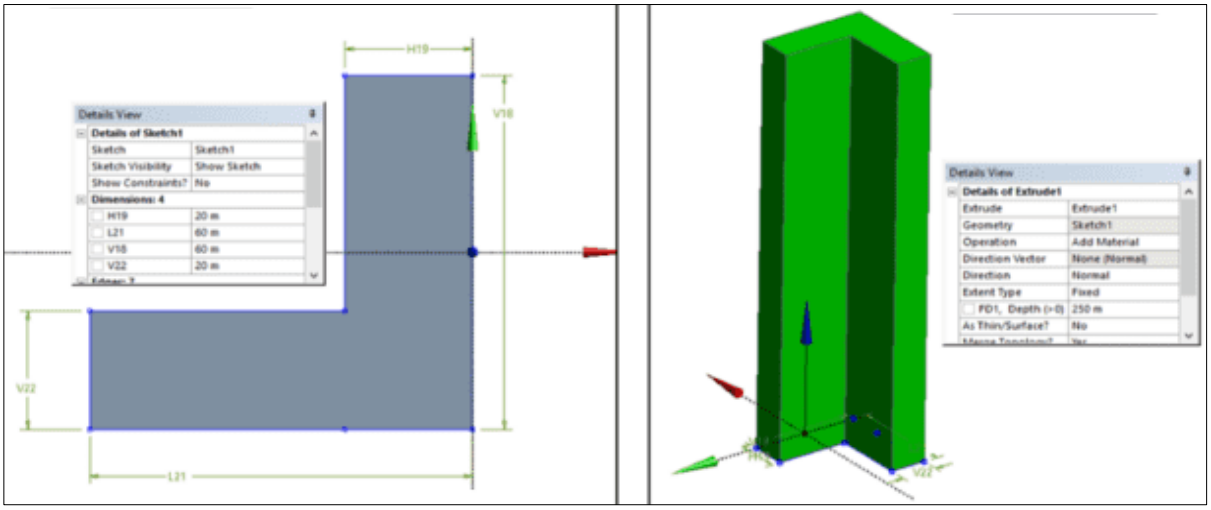

(b) L- shape

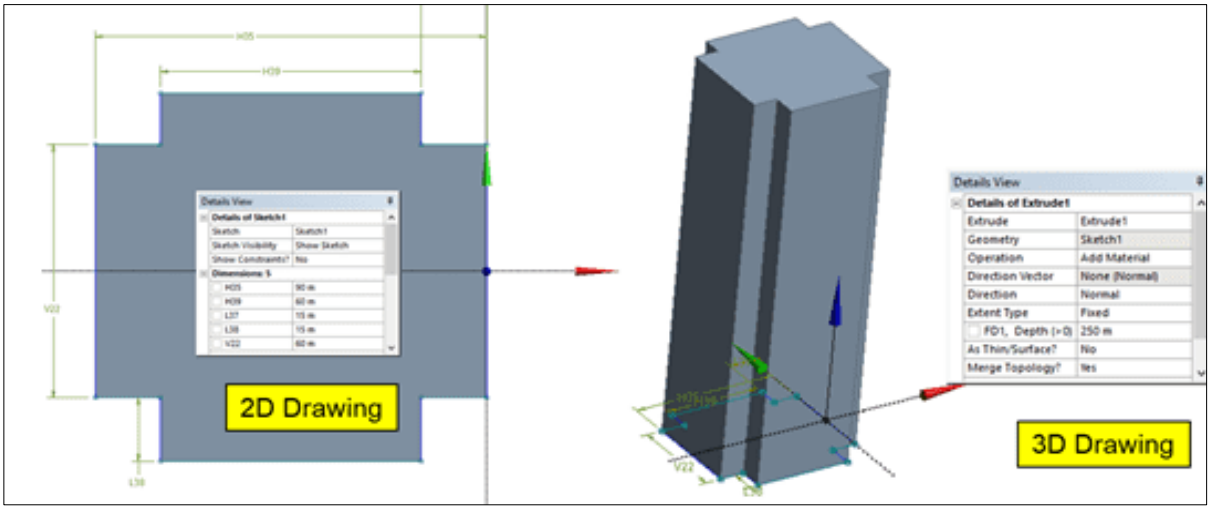

(c) Plus Shape

Fig. 2. Solid Model Geometry (a) Y- Shape (b) L- shape (c) Plus Shape

maximise kinetic energy efficiency,

$$\frac{\partial(\rho k)}{\partial t}+\frac{\partial(\rho k u_i)}{\partial x_i}=\frac{\partial}{\partial x_j}\left[\Gamma_k\frac{\partial k}{\partial x_j}\right]+\tilde{G}_k-Y_k+S_k \qquad (3)$$

The SST k-ω turbulence model Eq. (3), combined the advantages of the k-ε and k-ω models, while also addressing their limitations. The k-ω model accurately described boundary layer behaviour in the near-wall area, while the k-ε model often faced difficulties. In the outer flow zone, the SST model switched to the k-ε model for more precise forecasts. The hybrid approach enhanced the dependability and applicability of the SST k-ω model in comparison to its separate components. It balances precision and processing economy, making it a popular general-purpose turbulence model. The appropriateness of each turbulence model for different flow conditions and its accuracy-computational cost balance determined its usefulness. The selection of the model is being dependent on the flow characteristics and computing resources. The SST k-ω model has commonly been used as a default choice for undetermined flow characteristics. Researchers and engineers often opted for a model that met the simulation criteria in cases that called for specialised knowledge.

4. Numerical Model Development

In the field of computational fluid dynamics, a systematic approach is employed to solve the governing equations with a high level of precision and yield meaningful findings. First, inside the specified area, integrated partial differential equations expressing conservation principles, such as mass or momentum, over control volumes. This technique examined every control volume by using conservation laws. Integral equations were transformed into algebraic equations through the introduction of certain assumptions. This change simplified calculations. Iterative solutions are found for the nonlinear algebraic equations. The answer approached precision, a prerequisite for convergence, through iteration. A residual, or error, is generated with each repeat, which is used to measure the correctness of the flow characteristics. The layout, residual values, and dimensions of the control volume determined the accuracy of the

solution. Complex processes, such as combustion and turbulence, are approximated using empirical connections. The approximations used in these interactions resulted in a discrepancy between the CFD solution and the flow dynamics observed in the actual world. The iterative solution technique frequently achieved its goals with little to no human involvement, despite these obstacles. Following computations, the solver generated a comprehensive results file. A post-processor examined and displayed the file to gain a better understanding of the simulated fluid dynamics.

4.1. Geometric Modelling

Computational fluid dynamics approaches are currently used in research to accurately assess wind velocities, pressures, and forces exerted on tall buildings. The dimensions of the tall buildings under examination are displayed in Fig. 2 and 3. The buildings have Y-shaped, L-shaped, and 'Plus shape' cross-sections. To validate the model, a structure with a height of 250 m was used. The specifications of IS 875-2015 [13] were met, which specify the acceptable ranges of deflection for force, pressure, and velocity for both regular and irregular cross-sectional shapes. The Solid model showed a 250 m tall skyscraper with Y-shaped, L-shaped, and "Plus-shaped" cross-sections, as shown in Fig. 2 of the CAD design process. The CFD design modeler used a fluid domain measuring 300 x 600 m, which covered the whole structure. Within this domain, there were three separate sets of buildings, each measuring 250 m in height, as illustrated in Fig. 3. The fluid dynamics analysis takes into account wind directions at 0°, 90°, and 45°. All surfaces were composed of solid materials, featuring a smooth landscape with a "fixed" extension type. The CFD analysis is centered on the complicated geometry represented in Fig. 3, which comprises both fluid and solid components. The entrance of the fluid domain had dimensions of 300 x 400 m and a length of 600 m, highlighted the necessity for a thorough analysis of the interaction between fluid dynamics and solid structures.

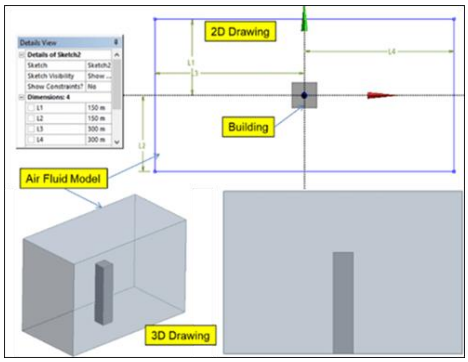

Fig. 3. Fluid-solid combined geometry

4.2. Meshing

A complete modeling tool was created with the successful development of the fluid-solid model, as shown in Fig. 4. Mostly, the achievement of precise and priceless results was through the use of computational fluid dynamics simulations. This tool achieved this by creating meshes and defining boundary conditions (BC). The tool enhanced the setup process, making it more thoughtful and thorough by highlighting the significance of boundary conditions. The quality and usefulness of the results were directly affected by using the right boundary conditions, making it an important step in ensuring the accuracy of the models. The numerous features of the simulation tool ensured that the CFD simulations ran on the fluid-solid model with increased accuracy and stability overall. The solid and fluid domains had a uniform total body size of 10m. A face size of 2 mm was employed to ensure accurate representation at the interface between the fluid and solid, hence enhancing precision through the formation of an expanding layer. The mesh contains a linear order element. As a result, a total of 735,868 elements and 250,297 nodes were generated. Fig. 4 exhibits the compound mesh configuration, facilitating a more thorough examination of the complex mesh structure.

4.3. Domains

Understanding air movement dynamics in a fluid region was essential to know air input. An extensive study was conducted to understand the behaviour, mobility, and interaction of air molecules in a specific region. The maintenance of a constant air temperature in the designated zone was crucial in this study. The temperature was kept at 25°C, providing a controlled setting for the study. The air pressure was set to 1 atmosphere, which allowed

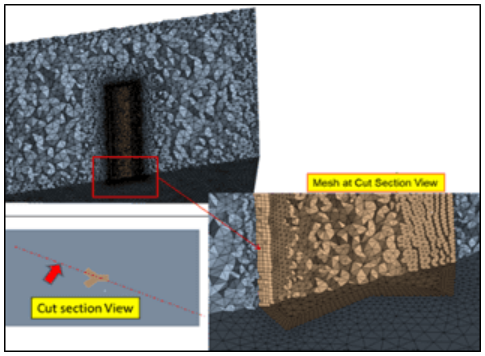

a) Y- Shape

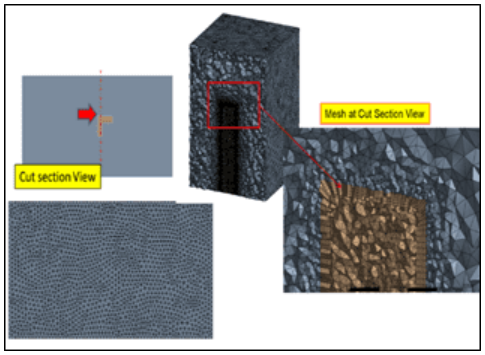

b) L-Shape

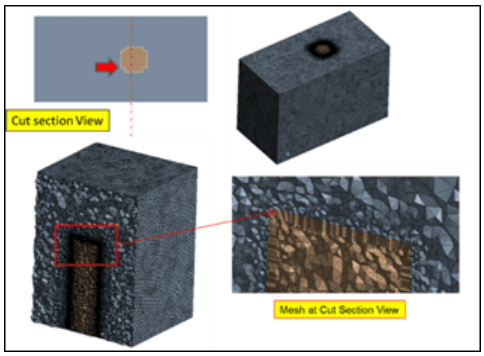

c) Plus Shape

Fig. 4. Mesh Details (a) Y- Shape (b) L- shape (c) Plus Shape

for the examination of how pressure influenced airflow. This ensured that outcomes were universally applicable. It was important to note that the study only covered a fixed, non-floating prototype. The research was simplified by focusing on fluid dynamics without movement or buoyancy. This focused method helps to explore the fundamental concepts that regulate air movement more thoroughly, improving understanding and forecasts. The size of the computer area plays a crucial role in determining the accuracy and usefulness of the results. Frank et al. [21] and Revuz et al. [22] provided useful statistics and a methodical approach to the investigation. Fig. 5 and Fig. 6 demonstrated the crucial role of domain identification in this particular case. Fig. 6 depicts a solid concrete construction. The continuous, static structure accurately resembled the solid area, much like a researcher would have observed in fluid dynamics.

4.4. Inlet

It is essential to pay great attention to the particulars of the inlet boundary conditions when analysing airflow. According to the information provided in Fig. 7, a predetermined normal speed of 50 m/sec is applied at the air-fluid inlet. In this particular instance, the study is carried out in the subsonic flow regime, more precisely with the Mass Momentum option. The behavior of the airflow at its typical speed is accurately characterised by this choice. For the purpose of realistically simulating the effects of turbulence inside the fluid domain, a turbulence option with a medium intensity of 5% has been included. Intake circumstances that are precise and properly described are necessary for it.

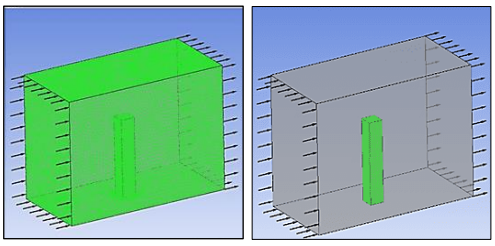

Fig. 5. Fluid Domain **Fig. 6.** Solid Domain

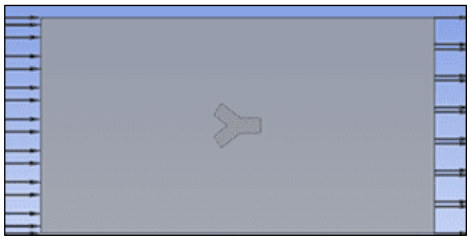

a) 0° Y- shape

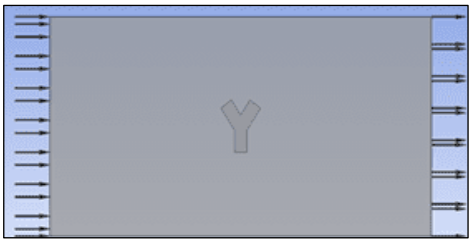

b) 90° Y- shape

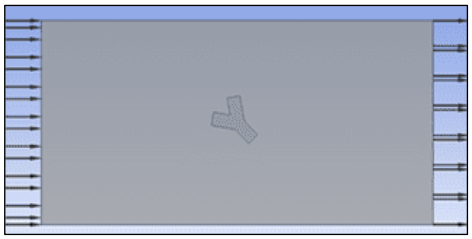

c) 45° Y- shape

Fig. 7. Inlet boundary condition

4.5. Outlet

The configuration of the air inflow investigation output is displayed in Fig. 8. The Mass Momentum option was utilised to determine the average static pressure. The pressure profile blend was 0.05, and the relative pressure was zero Pascal. Pressure-averaging was applied equally across the outflow to accurately analyse the subsonic air behaviour and qualities as it departed the location. The airflow dynamics analysis was made possible by utilising the Mass Momentum option and incorporating pressure averaging in the output configuration of Fig. 8. An understanding of the aerodynamic usefulness of the system was enhanced.

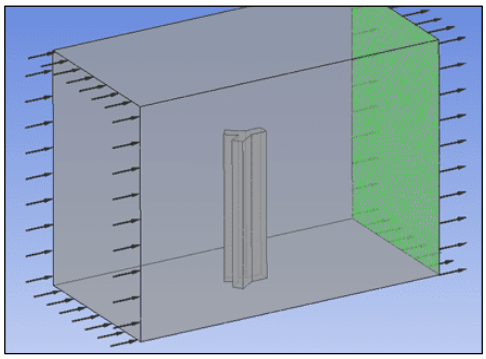

Fig. 8. Outlet boundary conditions

4.6. Solver Setting

Pressure was maintained at zero pascal to establish a reference point for atmospheric pressure, ensuring consistency in pressure measurement. A pressure profile blend of 0.05 allowed small pressure distribution changes to be fitted to unique simulation conditions or needs. The metrics provided a detailed assessment of air quality and behaviour after leaving the location, as well as airflow patterns and aerodynamic system performance. Fig. 9 provided a complete overview of the Solver Setting, while Fig. 10 illustrated the convergence test results for momentum and turbulence, showcasing their progression over time. Turbulence differed from momentum in that it described the disorderly motion of fluid particles within the flow, whereas momentum referred to linear velocity. The convergence patterns revealed system stability and efficiency. The data was plotted to reveal the interaction between momentum and turbulence over time.

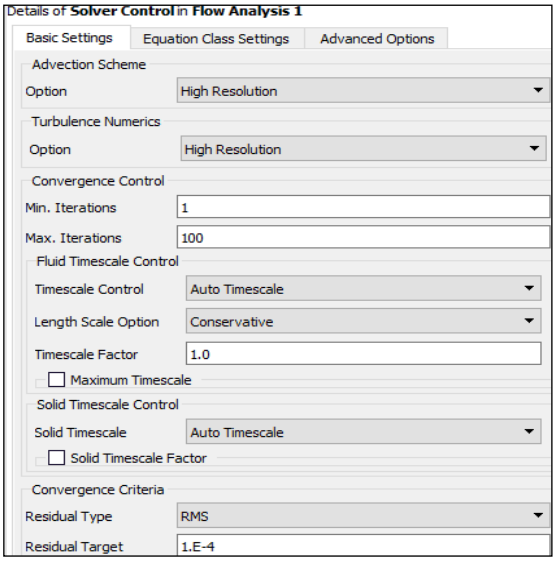

Fig. 9. Details of Solver Setting

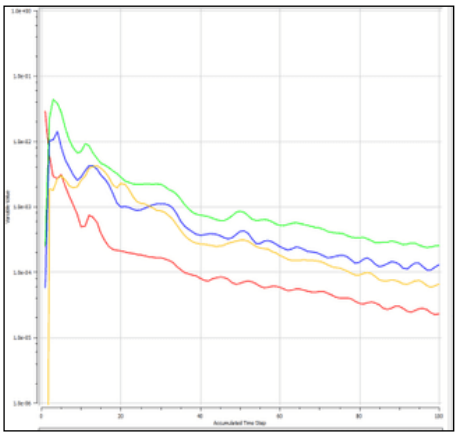

a) Number of iterations-100

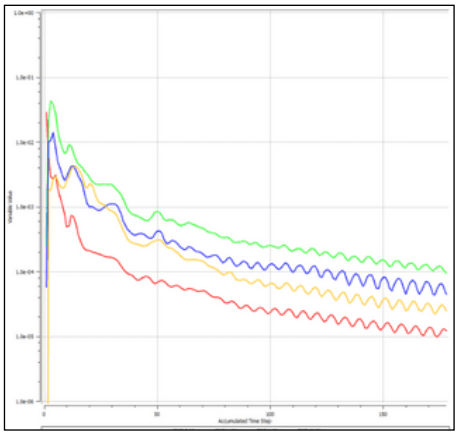

b) Number of iterations-200

Fig. 10. Momentum, Turbulence Convergence graph

This study investigated the impact of increasing the number of iterations in a computer simulation. The study emphasized factors such as maximum velocity and solution time. Despite doubling the number of repetitions from 100 to 200, the output velocity (Fig. 11) remained unchanged. However, the change was quite minimal, at a mere 0.2%. It was noteworthy to see that when the number of iterations was doubled, the computation time increased by 108%. However, it was seen that the shape of the velocity curve and its size followed the same pattern over 100 to 200 times. Based on the findings presented in Table 2. After careful analysis, it was concluded that conducting 100 iterations was sufficient for obtaining a stable answer without compromising accuracy.

Table 2. Iteration Precision and Efficiency

Parameters	***Initial Value***	***Final Value***	***% Change***
No. of iterations	100.00	200.00	100%
Max Velocity (m/s)	70.00	70.12	0.2%
Solution Time (Minutes)	39.00	81.00	108%

5. Results and Discussions

The simulation measured several important factors for a complete study. The data included velocity streamline, pressure contours, velocity contours, and the applied pivot force at different building heights. The simulation displayed height-dependent forces and pressures, unveiling fluid dynamics and structural interactions through meticulous variable assessment. A variety of methods were used to accurately evaluate the performance of the system and gave insights for improving design and structural integrity in varied conditions, making the research more important. The main topic of this study was the examination of the structural performance of structures with Y, L, and + shapes under various wind speeds. The understanding of the fluid dynamics and aerodynamics of each configuration was crucial to ensuring stability and maximising design efficiency, as each configuration presented its own set of challenges. Y, L, and + structure structural dynamics and aerodynamics were thoroughly examined. After that, the investigation examined how velocity angles affect different structures. The study investigated the impact of wind directions on Y-shaped buildings at 0°, 90°, and 45°. It also examined the aerodynamics and structural stability of L-shaped buildings and '+' shapes at wind angles of 0°, 90°, and 45°.

The study also explored how mesh density affected finite element simulation accuracy. Coarse and fine meshes were compared to determine the optimal mesh resolution for fluid-structure interaction. Strong buildings were constructed by those who understood the effects of wind. An extensive research was conducted to examine building layout and wind forces in order to enhance structural construction and durability. A total of eight samples were utilised to investigate real-time reactions to various mesh, wind orientations, and building designs.

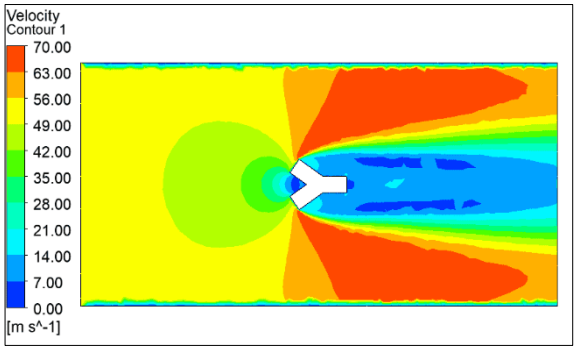

a) No of iteration-100

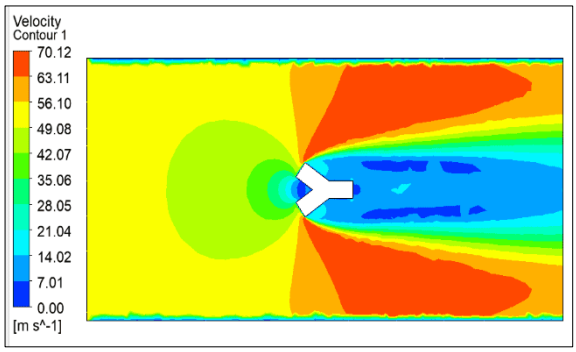

b) No of iteration-200

Fig. 11. Velocity path lines

5.1. The velocity Streamline

In this analysis, the wind was treated as a fluid, and streamlines were employed as mathematical tools to visually describe the speed of particle movement within the fluid. Streamlines are commonly utilised to examine both vertical and horizontal characteristics. The potential trajectories for particles suspended in the fluid are illustrated. Fig. 12 provides a top-down view of the building, illustrating the airflow patterns and velocity over the structure. This Fig. 12 also illustrates the speed distribution in a streamlined flow, provides insight into the direction of fluid particles in the area. The primary focus of the study was on buildings that exhibited non-uniform shapes. The purpose of this analysis was to assess the impact of wind direction at 0°, 90°, and 45° angles on Y-shaped structures in the first phase, L-shaped structures in the second phase, and '+' shaped structures in the third phase, with a specific focus on wind angles of 0° and 45°. Table 3 displays the highest velocities observed for the three types of building geometries and the proposed. Table 3 displayed the maximum velocities recorded for three different building designs when they were exposed to different wind directions. While observing Y-shaped buildings, the maximum velocity of 87.88 m/s was observed at an angle of 0 degrees. At an angle of 90 degrees, the speed experienced a notable decrease to 80.04 m/s. However, when the angle was set to 45 degrees, the speed remained relatively unchanged at 80.35 m/s. The velocity of L-shaped buildings reached its peak at 79.94 m/s when it was at an angle of 0 degrees. The velocity decreased to 77.89 m/s at a 90-degree

angle and then increased again to 80.04 m/s at a 45-degree angle. The building, shaped like a "+", reached its slowest speed of 85.04 m/s when it was at an angle of 0 degrees. It, then, accelerated to its highest velocity of 97.61 m/s when it reached an angle of 45 degrees. Every design has its distinct profile that interacts with the wind, leading to variations in aerodynamic performance. When the wind perfectly aligns with the central axis of Y-shaped structures, it led to higher speeds. However, any deviations from this alignment led to a decrease in airflow speed. Similarly, L-shaped structures experienced the highest velocities when the wind lined up with the longest side. The study clearly demonstrated the range of maximum velocities experienced by Y-shaped and L-shaped buildings when exposed to different wind angles. It was clear that these shapes were very sensitive to certain wind directions. It was observed that the building with a "+" shape gained speed when confronted with a 45-degree wind angle. It was clear that studying and improving aerodynamic performance while taking into account the shapes of the buildings and the direction of the wind was crucial.

5.2. Velocity contours at different heights

The data presented in Table 4 contained valuable information regarding the velocity characteristics at two distinct heights, specifically 200 m and 100 m. The data provided valuable insights into the extent of increased speed and the duration of speed fluctuations with respect to altitude. At an elevation of 200 m, there was a noticeable increase in the velocity magnitude when compared to the lower height of 100 m. This behaviour aligned with estimated outcomes, as elevated velocities at greater elevations were frequently linked to less surface friction and more exposure to unobstructed air currents. The visual data presented in Fig. 13 to 15 provided evidence that supported those results, demonstrating the patterns of velocity around tall buildings at heights of 100 m and 200 m. The velocity contours plotted at a height of 100 m in Fig. 13, 14, and 15 were instrumental in enhancing the understanding of the airflow around tall buildings. Fig. 13, 14, and 15 displays the contours of wind velocity at a distance of 200 m. observing increasing wind speeds around buildings was followed by a drop. The difference showed how buildings affected wind patterns, creating wind zones and velocity fluctuations. To understand urban wind behavior, it is important to note that wind speed tends to increase as altitude increases. Table 4 presents further evidence of the above-mentioned results, showcasing the maximum velocities for various types of buildings and impact angles at heights of 100 and 200 m. Upon examining

Table 3. Observed Maximum Velocity

Shape	***Y-shaped***			***L-shaped***			***'+' shaped***	
Angle (degrees)	0	90	45	0	90	45	0	45
Max. Velocity (m/s)	87.88	80.04	80.35	79.94	77.89	80.04	85.04	97.61

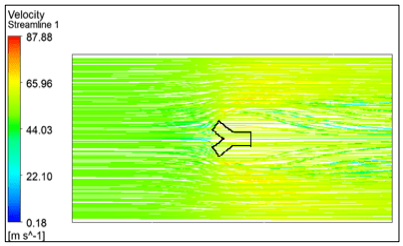

(a) 0° Y- shape

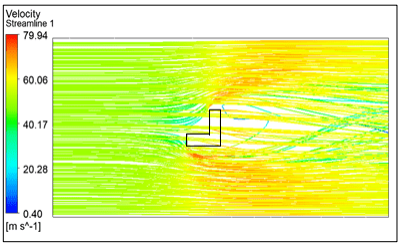

(b) 0° L- shape

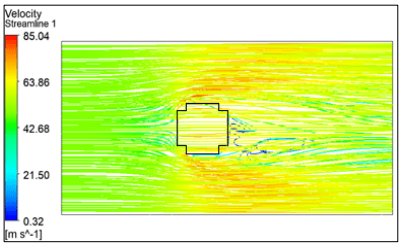

(c) 0° Plus-shape

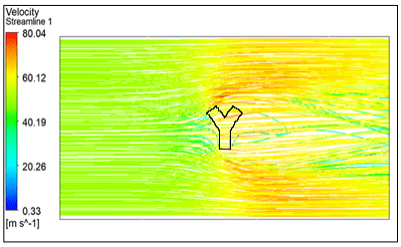

(d) 90° Y- shape

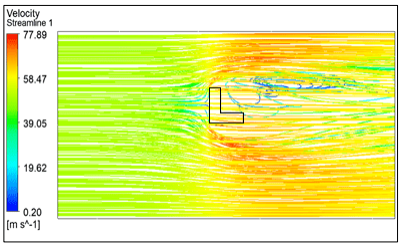

(e) 90° L- shape

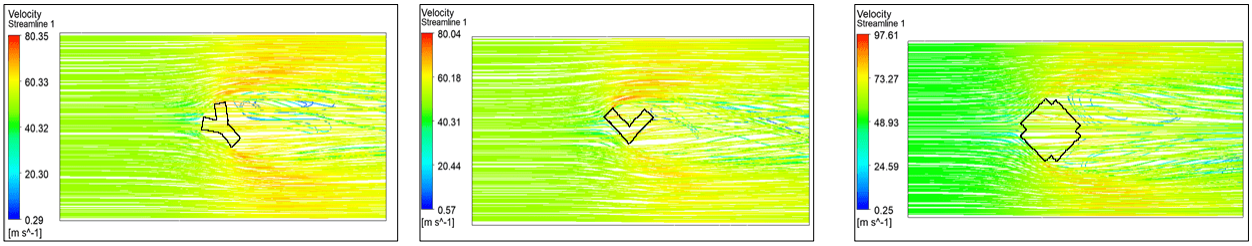

(f) 45° Y- shape (g) 45° L- shape (h) 45° Plus- shape

Fig. 12. Velocity path lines

how incidence angles varied across various building forms, the Y-shaped structure was found to have smoothly adjusted to shifts in wind direction, ensuring consistent wind speeds. On the other hand, the speeds of L-shaped and '+' shaped buildings exhibited more variation when viewed from different angles.

5.3. Pressure Contours of Building

From Fig. 16, it was observed that the wind moved at a speed of 50 m/s around the building. This observation was closely linked to the data shown in Table 5. This table documents the highest positive and negative pressures experienced by different building forms at different incidence angles. Significant patterns in pressure distribution were evident, indicating the notable impact of both the geometry of the structure and the angle at which the incident occurred. Table 5 illustrates the points at which airflow detaches from the building surface due to negative pressures. These phenomena arise from these events. The pressure fluctuations were caused by the distinctive structure and airflow patterns of the building. The study examined building forms and incidence angles to gain a full understanding of design and pressure distribution, and how they affect pressure patterns. With meticulous research, the study carefully recorded the highest positive and negative pressures encountered by different types of buildings at different angles of incidence, revealing significant patterns in pressure distribution. The patterns revealed how the shape of the structure affects pressure changes and building stability. The study also examined the impact of pressures on the structural stability and functionality in turbulent airflow. Through meticulous analysis of pressure profiles, a deeper understanding of the intricate relationship between the angle of incidence and pressure distribution has been uncovered. Understanding this complex process is facilitated by the discovery of both the highest positive and lowest negative pressures. The findings had a significant impact on building design and construction, enabling them to better withstand turbulent wind.

An investigation was conducted on pressure profiles in various building geometries and angles of incidence. The study finally highlighted the importance of understanding the impact of eddies, vortex shedding, and wake creation on airflow. This work aimed to enhance the considerate of design principles and structural

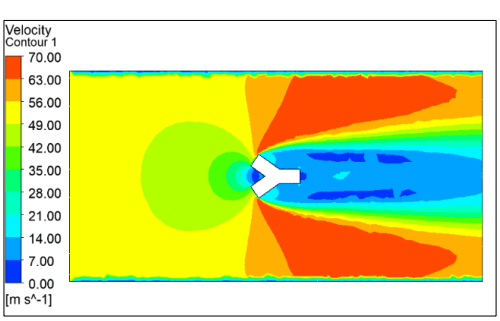

(a) Y- shape at 100 m height

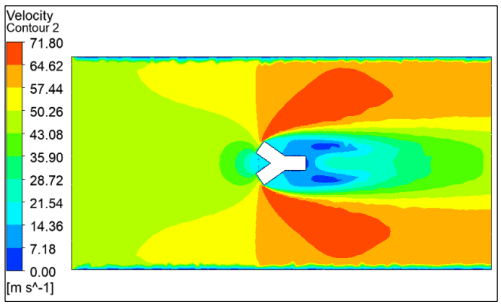

(b) Y- shape at 200 m height

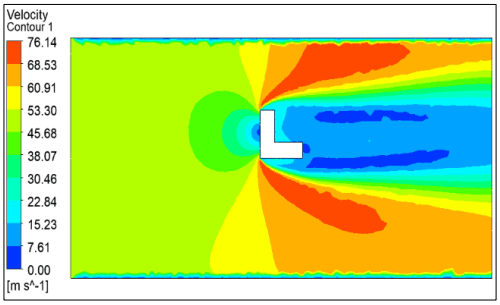

(c) L- shape at 100 m height

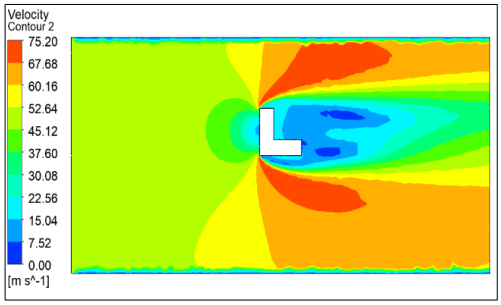

(d) L- shape at 200 m height

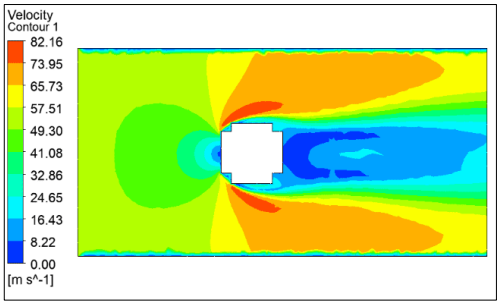

(e) Plus- shape at 100 m height

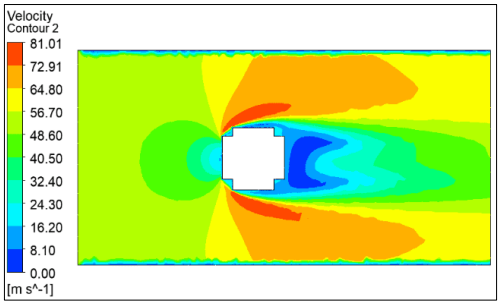

(f) Plus-shape at 200 m height

Fig. 13. Velocity Contours at 0°

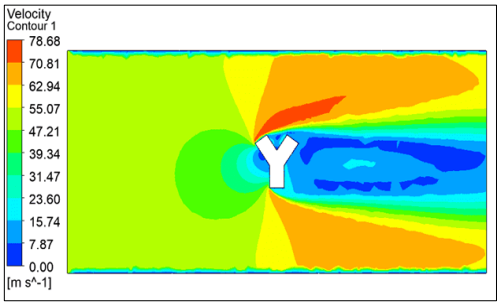

(a) Y- shape at 100 m height

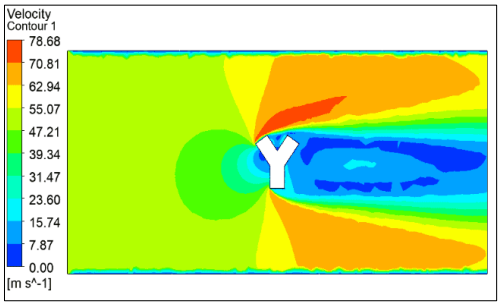

(b) Y- shape at 200 m height

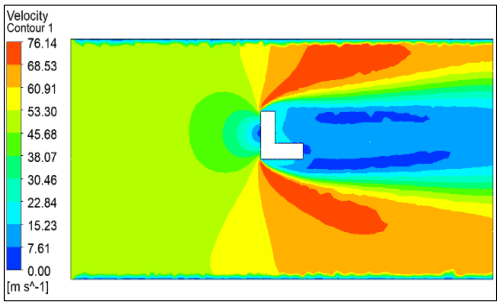

(c) L- shape at 100 m height

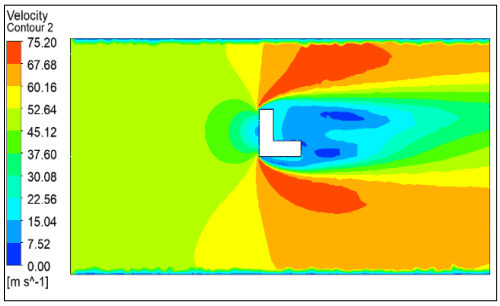

(d) L- shape at 200 m height

Fig. 14. Velocity Contours at 90°

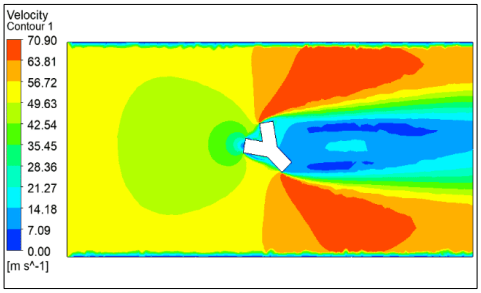

(a) Y- shape at 100 m height

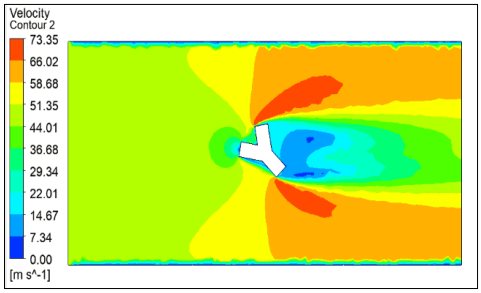

(b) Y- shape at 200 m height

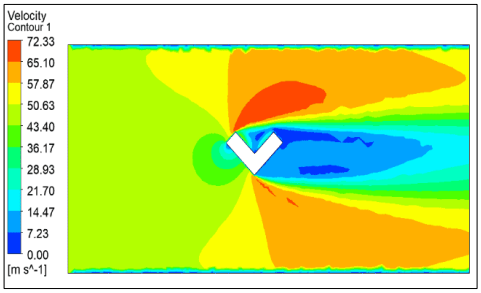

(c) L- shape at 100 m height

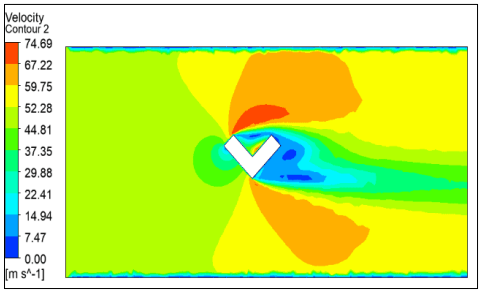

(d) L- shape at 200 m height

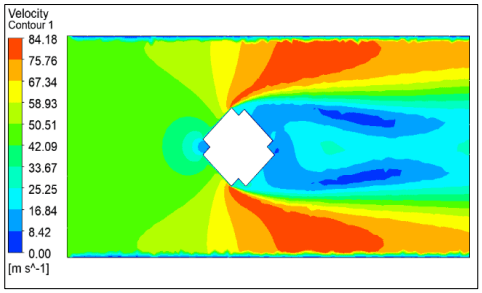

(e) Plus- shape at 100 m height

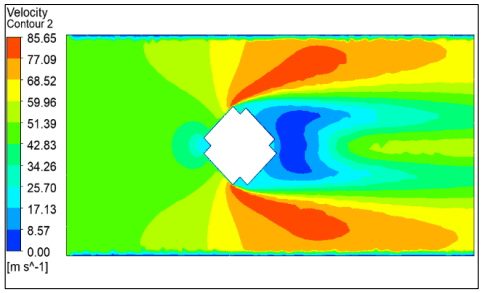

(f) Plus-shape at 200 m height

Fig. 15. Velocity Contours at 45°

Table 4. Velocities Contours

Shape	***Y-shaped***			***L-shaped***			***'+' shaped***	
Incident Angle (degrees)	0	90	45	0	90	45	0	45
Velocity in m/s at 100 m height	70.00	78.68	70.90	75.61	76.14	72.33	82.16	84.18
Velocity in m/s at 200 m height	71.80	77.34	73.35	74.82	75.20	74.69	81.01	85.65

Table 5. Pressure Profile Observed

Shapes	***Y-shaped***			***L-shaped***			***'+' shaped***	
Incident Angle (degree)	0	90	45	0	90	45	0	45
Max. Pressure (Pa)	2272.21	2339.48	2230.95	2289.56	2395.82	2018.31	2471.07	2967.97
Min. Pressure (Pa)	-5286.92	-4106.35	-4116.46	-3766.52	-2155.82	-5376.42	-4278.14	-6973.58

Table 6. Maximum Force Observed

Shapes	***Y-shaped***			***L-shaped***			***'+' shaped***	
Incident Angle (degree)	0	90	45	0	90	45	0	45
Force (N)	3.51E+07	4.05E+07	3.38 E+07	3.95E+07	4.11E+07	2.68 E+07	4.34E+07	6.93E+07

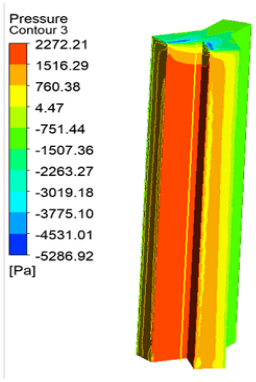

(a) 0° Y- shape

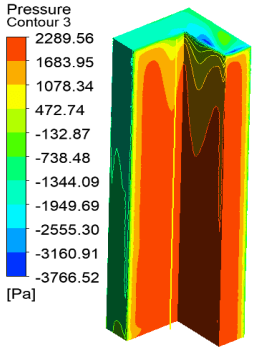

(b) 90° L- shape

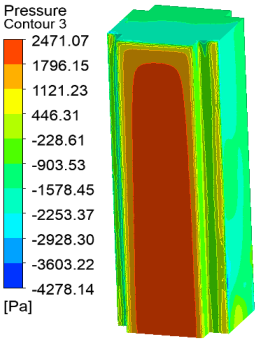

(c) 45° Plus- shape

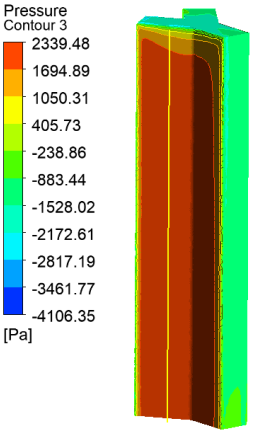

(d) 0° Plus- shape

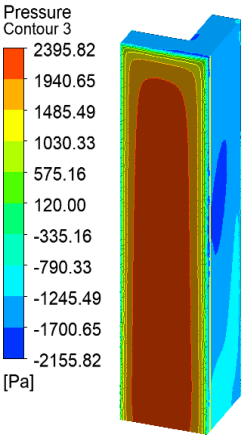

(e) 90° L- shape

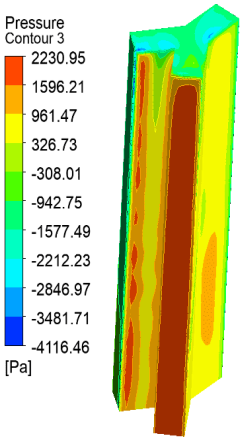

(f) 0° Y- shape

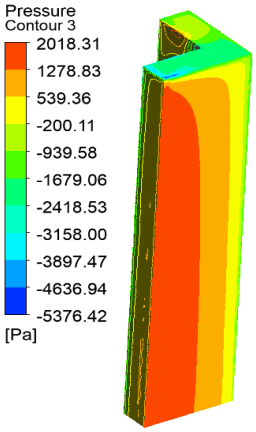

(g) 90° L- shape

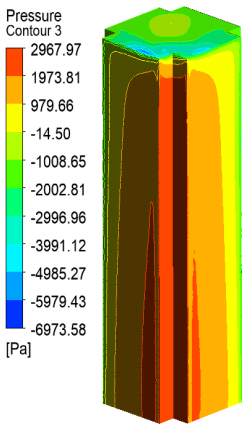

(h) 45° Plus- shape

Fig. 16. Pressure profile at building

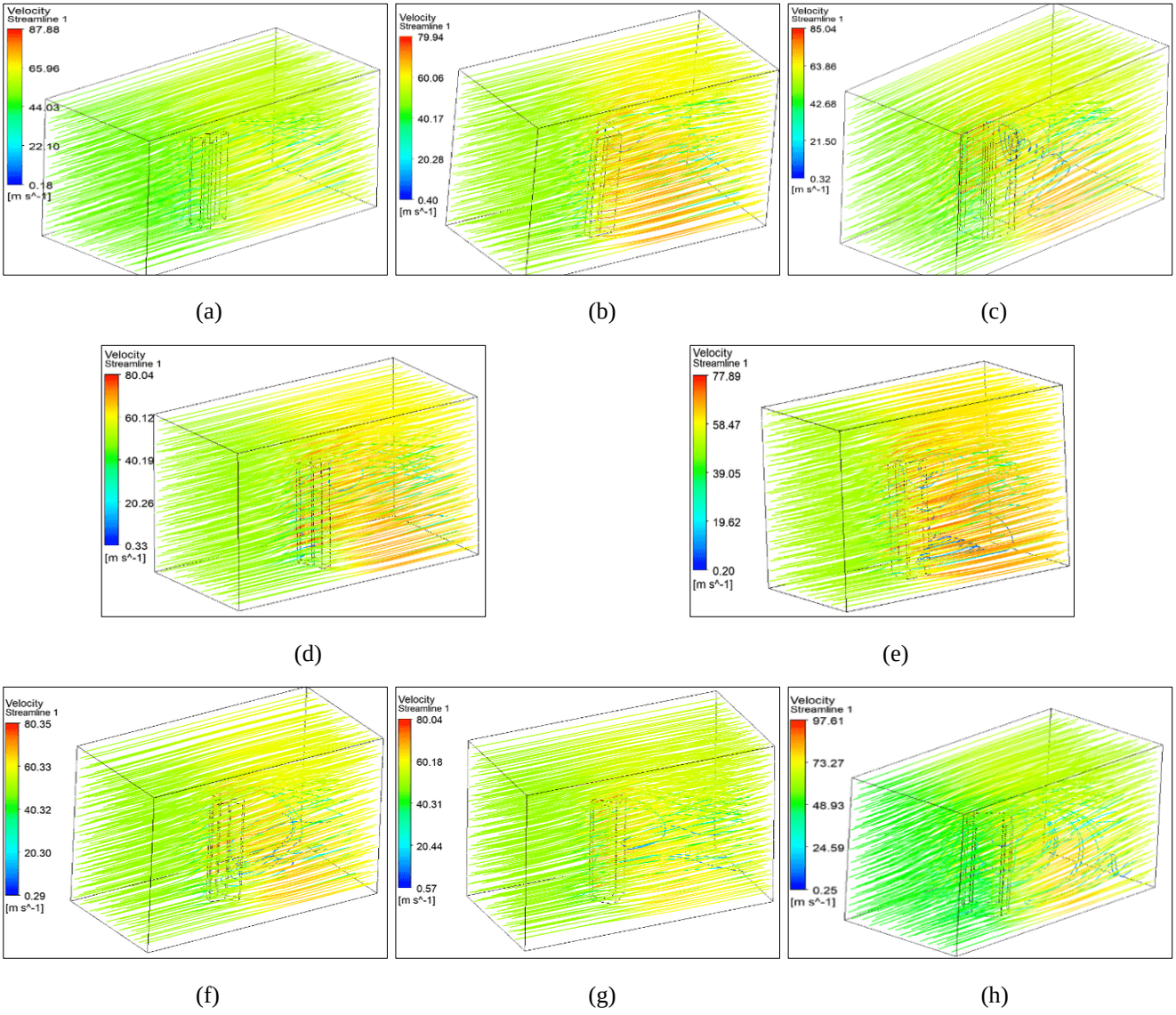

Fig. 17. Force acting on the building

stability in turbulent airflow conditions through the study of pressure patterns. A safe option when finalizing your figures is to strip out the fonts before you save the files, creating “outline” type. This converts fonts to artwork what will appear uniformly on any screen.

5.4. Force acting on the building

The findings of the study clarify how wind speed and impact angles affect buildings, as seen in Fig. 17. Table 6 accurately shows the maximum forces for Y-shaped, L-shaped, and '+'-shaped buildings at impact angles of 0, 90, and 45 degrees. The Y-shaped structure experienced a peak force of 4.05E+07 N when it was subjected to perpendicular wind, while the L-shaped structure produces a force of 4.11E+07 N. Whereas, the plus-shaped structure experiences the maximum force of 6.93E+07 N, from 45-degree wind. This study demonstrated that structural configuration and wind angle have a significant impact on wind forces. The Y and '+' shaped structures experienced significant force fluctuations due to the changes in wind direction and wind impact angles. Wind direction has the potential to impact these structures. The force applied to the L-shaped structure experienced a significant increase of 4.05% when the incidence angle was set at 90 degrees. The research advanced knowledge by improving the understanding of the complex interaction between wind, structural geometry, and stress.

5.5. Accuracy and Efficiency in Computational Simulations

A "mesh sensitivity study" examines how mesh resolution affects modeling results. Accuracy and efficiency are used

to evaluate effect of mesh reinforcement on simulation results. During the process of changing a mesh with moderate density to a finer density, changes in velocity were noted in the initial stage. The normal procedure involved modifying the number of mesh nodes and mesh elements to examine their impact on simulation results, such as maximum velocity and processing time.

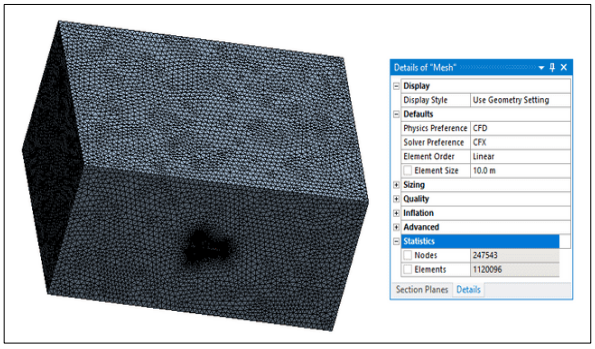

Fig.18. Moderate Mesh

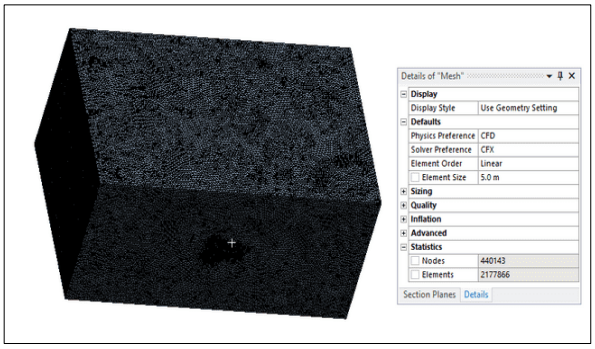

Fig.19. Moderate Mesh

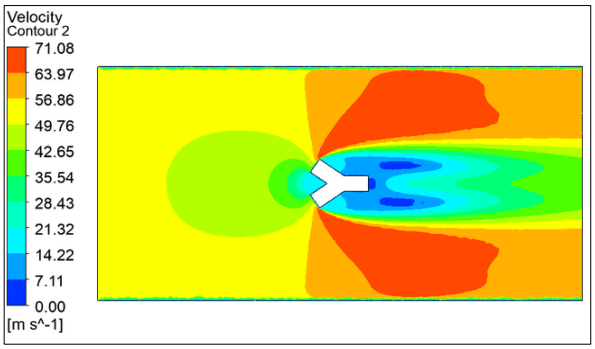

Fig. 20. Velocity path lines

Table 7. Mesh Sensitivity result summary

Parameters	***Moderate***	***Fine***	***% Change***
Mesh Node Count	247543.00	440143.00	78%
Mesh Element Count	1120096.00	2177866.00	94%
Max Velocity (m/s)	70.00	71.08	1.5%
Solution Time (Min)	39.00	104.00	167%

The summary Table 7 presented the results of a complete mesh sensitivity analysis, investigating the impact of mesh refinement on various param described in Fig. 18, Fig. 19 and Fig. 20. The transition from a moderate to a fine mesh had a significant impact on important param. There was a noticeable rise in the quantity of mesh nodes, going from 247,543 to 440,143, showcasing a percentage change of 78%. Similarly, there was a significant change in the quantity of mesh elements, as it rose from 1,120,096 to 2,177,866, indicating a 94% increase. The simulation had a minimal impact on the velocity. It increased by only 1.5% from 70.00 to 71.08 m/s. However, the time required to find a solution had a significant impact, rising from 39.00 to 104.00 minutes, indicating a considerable increase of 167%.The findings of this study highlighted the complex correlation between mesh refinement and computational output. The accuracy was improved by the finer meshes, but due to the significant increase in solution time, computational resources had to be carefully considered. This highlighted the importance of finding a balance between mesh refinement and simulation efficiency in real-world applications. Based on the above study, the chosen mesh proved to be sufficient for obtaining a clear illustration of the result.

5.6. Turbulence Model Selection and Considerations

When it comes to computational fluid dynamics simulations, the choice of turbulence model is of utmost importance as it has a direct impact on the accuracy of predictions and the computational expenses involved. The three patterns that were examined had advantages and disadvantages. The k-ε model was highly regarded for its simplicity and effectiveness, making it a popular choice for well-defined wall bounded flows with high Reynolds numbers.

However, this approach could have been ineffective in complex vortex or fragmented fluid dynamics scenarios. In complex fluid dynamics, such as split and whirling flows, the standard k-ω model outperformed the standard k-ε

model. The device demonstrated excellent performance close to obstacles and exhibited enhanced precision. The system encountered difficulties due to inadequate pressure gradients and unforeseen flow patterns. The SST k-ω model surpasses both the k-ω and k-ϵ Models in terms of effectiveness. The k-model accurately predicted the behavior of the boundary layer near barriers in the outer flow zone in this model. The technique is valuable in numerous scenarios because of its diversity, durability, accuracy, and cost-effectiveness. This method is highly effective for conducting generic turbulence simulations when the flow variables are not known. When selecting a turbulence model, it is crucial to take into account the simulated flow situation and processing capabilities. An objective assessment was conducted by considering the advantages and disadvantages of computation cost and accuracy, as carried out by experts and engineers. The performance of the SST k-ω model showed consistent improvement across different settings. However, on certain occasions, an alternative framework was required to accomplish goals.

6. Conclusion

An extensive analysis was conducted on the complex connection between the orientation of the geometry of a building and the impact of aerodynamic forces. This study investigated the maximum velocities, pressure distributions, and force production of different geometric shapes to reveal the aerodynamics of architectural structures. This paper explored a concise overview of the key findings of the study and its potential impact on structural design.

1. The alignment of the shape had a notable effect on both the maximum velocity and pressure. The maximum observed velocity was influenced by the location and shape of the building. At a temperature of 25 degrees, Y-shaped formations achieved a velocity of 87.88 m per second. The shape orientation had an impact on the distribution of pressure. A Y-shaped structure was built, resulting in a 0° angle that generated the highest peak pressure of 2272.21 Pa. It has been demonstrated that the orientation of a building in relation to the direction of the wind has a significant impact on aerodynamic forces.

2. Different shape provided dissimilar pressure profiles. Pressure measurements varied widely among structures, highlighting the role of shape geometry in aerodynamic forces. The pressure fluctuations ranged from -6973.58 Pa for the "+" configuration at 45 degrees to -2155.82 Pa for the "L" configuration at 90 degrees.

3. Irregularity in building shapes resulted in variations in the intensity of wind force applied. More complex designs, like the "plus" shape at a 45 degree angle, produced higher magnitudes of force (6.93E+07 N) compared to simpler shapes such as the Y shape at a 45 degree angle (2.68E+07 N). It was suggested that the complex geometric features of architectural structures had a substantial influence on the magnitude of aerodynamic forces experienced at high speeds.

4. The study has identified clear aerodynamic characteristics in geometries that were classified as Y, L, and +. The Y-shaped configuration at 0 degrees demonstrated the most efficient speed, while the "+" shape at 45 degrees exhibited the highest level of force. These observations highlighted the importance of fully understanding the variations in aerodynamic efficiency among different shape classifications to create more durable building designs.

5. Shapes with irregular geometries designs, like the + shape and a 45 degree wind angle, exhibited a higher velocity. The irregular structure showcased a noteworthy wind velocity of 97.61 m/s. The alignment of a shape in relation to the wind direction was of great importance. Shapes aligned with the direction of the wind and had a wind angle of 0 degree, which resulted in higher pressure. In this particular case, the pressure was recorded as 2272.21 Pa. Shapes that were aligned at a right angle to the wind (L: Shape-90 degree wind angle) experienced a reduction in pressure of -2155.82 Pa. An extra force of 6.93E+07 N was generated as a result of the discovery of irregular structures, especially those with a 45 degree shape. The degree of irregularity in the shape had a direct effect on the strength of the wind force. Y: Shape, at 0 degree wind angle, was the fastest, but it had less force than +: Shape, at 45 degree wind angle. There was a deeper connection between shape, orientation, and force that went beyond mere speed. Asymmetrical shape geometry led to varying levels of positive and negative pressure. Understanding the properties of each shape was crucial for analysing their impact on pressure and force.

The findings emphasized the importance of considering not only the magnitude of the forces but also their distribution across different building shapes. When designing buildings in regions that were prone to high wind velocities, engineers and architects had to take into consideration the orientation of the structures as well as the complexity of the structures. This was done to minimise any potential structural weaknesses that have been present.

Funding Declarations

The authors declare that they have no known competing financial interests or personal relationships that could have appeared to influence the work reported in this paper.

Conflicts of interest

The authors declare that there is no conflict of interest regarding the publication of this paper.

References

[1] Pal, S., Raj, R., and Anbukumar, S. “Bilateral

interference of wind loads induced on duplicate building models of various shapes." Latin American Journal of Solids and Structures, Vol. 18, 2021, pp. 1–27. https://doi.org/10.1590/1679-78256595

[2] Verma, S. K., Ahuja, A. K., and Pandey, A. D. "Effects of wind incidence angle on wind pressure distribution on square pan tall buildings." Journal of Academic Industrial Research, Vol. 1, No. 12, 2013, pp. 747–752.

[3] Bhattacharyya, B., and Dalui, S. K. "Comparative study between regular and irregular plan shaped tall building under wind excitation by numerical technique." Proceedings, National Conference on Innovation in Design and Construction Industry Structures, 2014, pp. 10–15. http://dx.doi.org/10.13140/2.1.1689.9202

[4] Yadav, V., and Amin, J. A. "CFD Simulation on a Group of Tall Buildings." In Recent Advances in Civil Engineering for Global Sustainability, (RACEGS), 2016, pp. 309–316.

[5] Blocken, B., Janssen, W. D., and van Hooff, T. "CFD simulation for pedestrian wind comfort and wind safety in urban areas: General decision framework and case study for the Eindhoven University campus." Environmental Modelling & Software, Vol. 30, 2012, pp. 15–34

[6] Calzolari, G., Liu, W., "Deep learning to replace, improve, or aid CFD analysis in built environment applications: A review. Building and Environment", 206, 108315, 2021, pp. 1–12.

[7] Harman DHS, "Analysing the Effect of Cross-Sectional Change of Column on Symmetrical RCC Frame Structure", International journal of engineering sciences & research technology (IJERT), 6:06, Vol. 6, 2017, pp. 381–386.

[8] Kim, Y. M., and You, K. P., "Dynamic responses of a tapered tall building to wind loads", Journal of wind engineering and industrial aerodynamics, 90(12-15), 2002, pp. 1771-1782.

[9] Ding, F., and Kareem, A. "Tall buildings with dynamic facade under winds." Engineering, Vol. 6, No. 12, 2020, pp. 1443–1453. https://doi.org/10.1016/j.eng.2020.07.020

[10] Karimimoshaver, M., Hajivaliei, H., Shokri, M., Khalesro, S., Aram, F., and Shamshirband, S., "A model for locating tall buildings through a visual analysis approach." Applied Sciences, Vol. 10, No. 17, 6072. 2020, pp. 1-25. https://doi.org/10.3390/app10176072

[11] Fuka, V., Xie, Z.-T., Castro, I. P., Hayden, P., Carpentieri, M., and Robins, A. G. "Scalar fluxes near a tall building in an aligned array of rectangular buildings." Boundary-layer meteorology, Vol. 167, 2018, pp–53–56. https://link.springer.com/article/10.1007/s10546-017-0308-4

[12] Longarini, N., Cabras, L., Zucca, M., Chapain, S., and Aly, A. M. "Structural improvements for tall buildings under wind loads: comparative study." Shock and Vibration, 2017, pp. 1–19. https://doi.org/10.1155/2017/2031248

[13] IS 875 (Part-3) (2015) Design Loads (Other than Earthquake) for Buildings and Structures - Code of Practice Part 3 Wind Loads, Bureau of Indian Standards, New Delhi, India

[14] Sevalia, J., Desai, A., and Vasanwala, S. A. "Effect of geometric plan configuration of tall building on wind force coefficient using CFD." International Journal of Advanced Engineering Research and Studies, Vol. 1, 2012, pp. 127–130.

[15] Hemida, H., and Šarkić, A. "Wind Tunnel Tests-air Flow around Buildings, Final Report of the Short Term Scientific Mission as part of the COST Action." TU1304, 2014.

[16] Feras, A. L. Z., LI, Z., WEI, Q., and SUN, Y. "Wind tunnel test and numerical simulation of wind pressure on a high-rise building." Journal of Chongqing University (English Edition), Vol. 1, 2010, pp. 1–24. http://dx.doi.org/10.1155/2020/8850688

[17] Wijesooriya, K., Mohotti, D., Lee, C. K., and Mendis, P. "A technical review of computational fluid dynamics (CFD) applications on wind design of tall buildings and structures: Past, present and future", Journal of Building Engineering, Volume 74, 106828, 2023, pp. 1–25.

[18] Abu-Zidan, Y., Mendis, P., and Gunawardena, T. "Optimising the computational domain size in CFD simulations of tall buildings." Heliyon, Vol. 7, No. 4, 2021, pp. 1–13. https://doi.org/10.1016/j.heliyon.2021.e06723

[19] Kumar, A., and Raj, R. "Study of pressure distribution on an irregular octagonal plan oval-shape building using CFD." Civil Engineering Journal, Vol. 7, No. 10, 2021, pp. 1787–1805.. http://dx.doi.org/10.28991/cej-2021-03091760

[20] IS 1893 (Part-1) (2016) Criteria for Earthquake Resistant Design of Structures Part-1 General Provisions and Buildings (Sixth Revision). Bureau of Indian Standards, New Delhi, India

[21] Franke, J., Hirsch, C., Jensen, A. G., Krüs, H. W., Schatzmann, M., Westbury, P. S., Miles, S. D., Wisse, J. A., and Wright, N. G. "Recommendations on the use of CFD in predicting pedestrian wind environment." The Fourth International Symposium on Computational Wind Engineering, (Vol. 14), 2004.

[22] Revuz, J., Hargraves, D., and Owen, J. "Domain size for computational fluid dynamics modelling of tall buildings." 9th UK Conference on Wind Engineering, 2010, pp. 273–276.